At-wavelength alignment and testing of the 0.3 NA MET optic

Kenneth A. Goldberg, Patrick P. Naulleau, Paul E. Denham, Senajith B. Rekawa, Keith Jackson, Erik H. Anderson, and J. Alexander Liddle
Center for X-Ray Optics, Lawrence Berkeley National Laboratory, Berkeley, California 94720

(Received 2 June 2004; accepted 21 September 2004; published 10 December 2004)

Extreme ultraviolet (EUV) interferometry has been successfully performed for the first time at 0.3 numerical aperture (NA). Extensive EUV "at-wavelength" testing including alignment, was performed on a newly created Micro Exposure Tool (MET) optic designed for sub-50-nm EUV lithographic imaging experiments. The two-mirror, 0.3 NA MET is among the highest resolution light-projection lithography tools ever made. Using both lateral shearing and phase-shifting point-diffraction interferometry, the wavefront was measured across the field of view, and the alignment was optimized in preparation for imaging. The wavefront quality reached 0.55 nm RMS ($\lambda_{EUV}/24.5$) in a 37-term annular Zernike polynomial series, dominated by higher-order spherical aberration. Measurements included calibrations of the interferometer accuracy, assessment of repeatability, and cross-comparisons of visible and EUV interferometric measurements. © *2004 American Vacuum Society.* [DOI: 10.1116/1.1815303]

I. INTRODUCTION

A new generation of 0.3 numerical aperture (NA), 5× demagnification, prototype extreme ultraviolet (EUV) optical systems is being produced to provide an opportunity for early learning with sub-50-nm imaging. Our research goals include the evaluation of advanced photoresist formulations and innovative EUV reticle technologies. Developed for static microfield imaging, these two-mirror, 0.3 NA, Micro-Exposure Tool (MET) optics operate at 13.5-nm wavelength, and have a design Rayleigh resolution of 27-nm.[1–3] They hold the promise of even higher resolutions achieved with tailored illumination conditions.[4] Visible-light and EUV wavefront measurements of the MET reveal it to be one of the highest resolution light-projection lithography tools ever made.

In order to achieve optimal, diffraction-limited performance, EUV optical systems require alignment to subnanometer aberration tolerances. Wavefront aberrations of a few tenths of a nanometer can cause a significant reduction in the process window. While image-printing and certain aerial image monitoring configurations will provide some wavefront quality feedback, at these small features sizes, near the limits of current photoresist resolutions, detailed quantitative system measurements are only available from interferometry. Ultrahigh-accuracy interferometry is a cornerstone requirement for the success of these and future optics, and represents a strategic risk-reduction step for these expensive developmental optics. Operating at the design EUV wavelength, EUV interferometry has been used in the diagnosis and remediation several types of fabrication and system-alignment errors, in the assessment of chromatic effects and flare, and most importantly, in the optimization and modeling of imaging performance.[5–9]

For EUV optics, the required system wavefront accuracies approach or exceed the accuracy limits of the interferometers used to test them. Active collaborations between researchers at Lawrence Livermore National Laboratory (LLNL) and Lawrence Berkeley National Laboratory (LBNL), in the co-operative measurement of nine prototype EUV optics, have improved our confidence in ultrahigh accuracy interferometry in the 100-pm domain. Careful intercomparisons have led to the discovery and remediation of several systematic error sources that would have been difficult to diagnose in isolation. Such an opportunity was available in one of the MET optics, which was aligned and measured at LLNL before being brought to LBNL for continued alignment in preparation for imaging.

This MET optic has been subjected to extensive interferometric testing. At the conclusion of visible-light alignment, the system was transferred to the Advanced Light Source (ALS) at LBNL where an EUV interferometer is installed on an undulator beamline. The EUV interferometer and the results of visible light alignment are described in Refs. 2 and 3. Before shipping, careful measurements were made of the conjugate point positions; coordinate transfer was facilitated by a metrology tower comprised of in-vacuum CCD cameras and capacitance micrometers.

Several different EUV interferometry techniques have been under development at LBNL since 1993. Testing the MET optic, with its high (annular) 0.3 NA presented the greatest challenge to date. Although its field of view is relatively small (600×200 μm), the numerical aperture is three times higher than that of the previous generation of EUV lenses. Systematic errors in the interferometer arise from the testing geometry and the relative alignment of the optical components; error magnitudes scale as powers of the NA. This makes calibration measurements at 0.3 NA many times more important and difficult than similar measurements at 0.1 NA. These systematic effects were measured and compensated using newly developed null-testing techniques which are beyond the scope of this article.

We report the results of EUV interferometry in two different configurations: cross-grating lateral shearing interferometry, and phase-shifting point-diffraction interferometry.

In addition to the alignment, system stability is discussed, and an intercomparison with visible-light interferometry is presented.

II. WAVEFRONT MEASUREMENTS AND ALIGNMENT

High-accuracy wavefront measurements facilitate system optimization for high-resolution imaging. Alignment of the MET is performed by the actuation of a six-arm mount on the small, convex, primary mirror, M1, and by the repositioning of the conjugate points in three-dimensions. The arm motion is driven by Picomotors which are designed for long-term stability when not in use. The most sensitive wavefront aberrations to arm actuation are coma, astigmatism, and spherical aberration, in that order. The actuation of any single arm introduces roughly equivalent amounts of coma with a RMS magnitude of approximately 3.0 nm per μm of actuation. The same amount of actuation introduces approximately 0.17 nm of astigmatism, and 0.07 nm of spherical aberration.

The optic is designed to have a wafer-side field of view of $600\times 200\ \mu$m, 3×1 mm on the reticle-side, within tilted conjugate planes. A 4° reticle-plane tilt allows light reflected from the reticle to enter the optic parallel to the central axis of this rotationally symmetric system. Respecting the tilted conjugate planes (4° reticle, and 0.8° wafer), measurements were performed across a three-dimensional volume field of view; up to 27 points were measured per data set. The aberrations vary within the field, and the most significant dependencies are (approximately): 0.08 nm astigmatism, and 0.06 nm spherical aberration per mm of lateral displacement; and 0.10 nm coma and 1.66 nm spherical aberration per mm of longitudinal displacement (RMS aberration magnitudes). The 4° reticle tilt introduces a reticle-side longitudinal position change of $\pm 35\ \mu$m across the narrow direction of the field, which adds ±36 pm RMS of spherical aberration.

The annular pupil shape, including the four narrow "spider" obstructions, requires us to describe the wavefront using a basis set of aberration polynomials that is orthogonal on the measurement domain. Derived from the Zernike circle polynomials, these aberration terms form a proper basis for the alignment and characterization of the optical system. The quoted aberration coefficients always refer to such a basis, although slightly different basis sets are used for different measurements and comparisons where more or less of the pupil domain is included. For annular pupils in general, differences between coefficients of the orthogonal basis and the conventional Zernike circle polynomials can be significant, especially for the spherical aberration terms.

Wavefront measurements were performed at a controlled temperature of 20.0 °C, in a vacuum environment with a base pressure of 1×10^{-7} Torr. A partial pressure of oxygen gas at 4×10^{-5} Torr was introduced as a preventive measure, to mitigate carbon contamination of the pinholes.

A. Predicted system wavefront

Prior to assembly, the individual mirror elements were measured by Carl Zeiss, and separately, mirror M1 was measured by LLNL. Based on the initial individual mirror wavefronts, the system wavefront at the central field point was predicted to have a RMS wavefront aberration magnitude of 0.17 nm in the first 37 Zernike terms. However the LLNL measurement of M1 showed the presence of a higher-order spherical aberration with an aberration magnitude of 0.22 nm, which in reflection could contribute 0.44 nm to the total system wavefront.[3]

B. Visible-light measurement

At the conclusion of visible-light alignment, the total system wavefront error was 0.56 nm RMS in a 37-term annular Zernike series, dominated by 0.49 nm of higher-ordered spherical aberration; close to the value predicted by the LLNL M1 single-element testing. The astigmatism, coma, and spherical aberration were reduced to 0.15, 0.10, and 0.05 nm respectively.[3] The visible-light measurements cover a limited radial subdomain of the full pupil: 10–26 mm radius out of a full pupil radius of 8.4–27 mm, or 87% of the full area. Reductions of the measurement domain can lead to an underestimation of the full pupil's wavefront aberration magnitude; thus comparisons are performed on identical domains.

C. EUV interferometry methods

Foucault, or knife-edge testing, is performed as the initial step in shearing interferometry. These tests unambiguously indicated the presence of higher-order spherical aberration.

For quantitative wavefront measurements, two very different EUV interferometry methods were used: lateral shearing interferometry (LSI), using a cross-grating configuration,[2,10] and phase-shifting point-diffraction interferometry (PS/PDI).[2,11] There are specific advantages and disadvantages to each technique.

1. Lateral shearing interferometer

Owing to its ease of alignment and tolerance for larger wavefront errors, the LSI was the primary measurement method. A two-dimensional "cross" grating is placed in the first Talbot plane beyond the focal plane. Several different gratings were available on an image-plane mask; our most common configuration was a 1.5-μm-pitch grating placed 76.9 μm beyond the focal plane, producing approximately 32 fringes across the pupil. Shearing is a self-referential technique that relies on the interference of the test beam with displaced copies of itself. As such, regions adjacent to any pupil boundary must be excluded, and the measurement area is reduced by approximately 3%. Analysis of the interference pattern produces approximations to the wavefront gradient in two perpendicular directions simultaneously. Reconstruction of the original test wavefront is performed using zonal[12] and modal[13,14] techniques, and both reconstruction methods were employed during the measurements. We are still evaluating

TABLE I. Wavefront measurements spanning nine positions within the 600×200 μm field of view, from 3 separate days. Each point represents the average of 4 or 5 independent measurements made at a given field position. The total 37-term RMS wavefront error is given at left; the RMS magnitudes of other important aberration coefficients are also given.

σ_{37} RMS	Astigmatism	Coma	Spherical ab.	Trifoil	Higher-order Spherical ab.
July 2, 2003: Initial measurement (nm)					
1.04 1.23 1.22	0.05 0.47 0.11	0.24 0.55 0.56	0.82 0.82 0.86	0.12 0.19 0.16	0.37 0.36 0.38
1.15 1.19 1.32	0.24 0.29 0.21	0.32 0.45 0.70	0.89 0.86 0.85	0.13 0.09 0.12	0.37 0.38 0.37
1.27 1.23 1.31	0.29 0.43 0.42	0.60 0.34 0.50	0.84 0.94 0.96	0.12 0.10 0.05	0.37 0.38 0.37
September 25, 2003: Optimized alignment (nm)					
0.79 0.59 0.71	0.56 0.12 0.26	0.10 0.12 0.24	0.07 0.05 0.24	0.13 0.13 0.12	0.37 0.36 0.37
0.90 0.55 0.76	0.59 0.04 0.19	0.37 0.06 0.36	0.01 0.04 0.36	0.19 0.14 0.12	0.38 0.37 0.36
0.71 0.60 0.61	0.38 0.25 0.13	0.23 0.11 0.14	0.01 0.02 0.14	0.12 0.12 0.11	0.37 0.36 0.36
October 24, 2003: The final field measurement (nm)					
1.16 1.00 0.99	0.72 0.07 0.28	0.73 0.80 0.69	0.02 0.16 0.06	0.18 0.09 0.12	0.36 0.36 0.36
1.22 0.80 0.94	0.41 0.07 0.39	0.96 0.56 0.52	0.01 0.08 0.04	0.18 0.15 0.11	0.38 0.36 0.37
0.83 0.76 0.83	0.48 0.03 0.30	0.34 0.51 0.49	0.03 0.04 0.03	0.15 0.08 0.23	0.37 0.37 0.37

the advantages and error sensitivities of these methods; typically the discrepancies were on the order of 0.05 nm or smaller for individual aberration coefficients.

2. Phase-shifting point-diffraction interferometer

Using diffraction from a pinhole in the image plane, the PS/PDI offers direct wavefront measurement through comparison of the test beam with a spherical reference wavefront. We regard the PS/PDI as the accuracy standard for our EUV wavefront measurements. However, relevant pinhole sizes for PS/PDI testing at 0.3 NA are between 20 and 35 nm.[2,3] With Ni as the absorber material of choice, mask opacity requirements necessitate the use of 150–200-nm-thick films, making pinhole fabrication a significant challenge. Furthermore, the alignment of the interferometer requires 10–15 nm lateral pinhole positioning, 100 nm longitudinally. This small capture range is reduced in the presence of wavefront aberrations whose magnitude decreases the Strehl ratio and lowers the available peak intensity at focus.

PS/PDI pinhole masks were fabricated using the Nanowriter, an electron-beam lithography tool at the Center for X-Ray Optics (CXRO), LBNL. The potentially-low transmission efficiency of small pinholes raises the opacity requirements of the mask, necessitating the use of a thicker absorber layer, and compounding the difficulties of pinhole fabrication. Pinholes used in the experiment were fabricated in 140-nm-thick, free-standing Ni membranes.[2,3]

D. EUV wavefront measurements

Over the course of several months, thousands of individual wavefront measurements were made. Using LSI, the wavefront was measured across the field of view eleven separate times. The most significant of those measurements are: (1) the first measurement at 20.0 °C, which enables comparison with the final visible-light measurement (July 2, 2003); (2) the optimized alignment, which shows the highest achieved wavefront quality (September 25, 2003); and (3) the final alignment state of the optic, measured one month after the final alignment procedure (October 24, 2003).

When LSI was used to measure the wavefront across the field of view, measurements were made at nine or more separate points, covering the corners, edges, and center of the field within the tilted conjugate planes. Aberration coefficients from three wavefront measurement sets are shown in Table I, and are discussed below. These coefficients describe the field variation of the wavefront aberrations on the three occasions mentioned above.

1. First EUV LSI measurement, and visible-light PSDI comparison

Figure 1(a) shows a side-by-side comparison of system wavefronts at the same position, close to the central field point. Both measurements were made with the system at a stable temperature of 20 °C. The EUV wavefront contains a large, unexpected, primary spherical aberration (0.80 nm RMS). The significant measurement differences are on the order of 1 nm—as large as the wavefront error itself. With this limited data, the differences cannot be specifically attributed to differences between the two interferometers nor to changes in the system alignment that may have occurred during shipping and installation—both are possible explanations. In fact, abrupt changes in the spherical aberration magnitude were observed on several occasions during EUV interferometry.

While primary spherical aberration is the most significant difference, other differences appear, including terms that are not related to the alignment, such as trifoil. When the spheri-

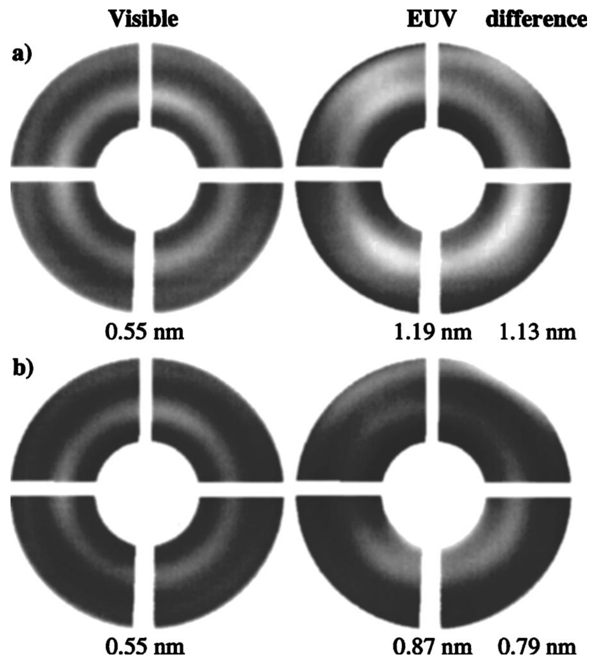

FIG. 1. Comparison of the final visible-light wavefront measurement with the first EUV measurement made at the same temperature, 20.0 °C. Wavefronts shown are 37-term fits reconstructed on the smaller pupil domain used visible-light interferometry. This EUV LSI measurement was made prior to alignment (a) Spherical aberration and coma dominate the difference. (b) With spherical aberration removed, the higher-ordered spherical aberration common to both becomes more apparent. Specific differences for some aberration terms and the total wavefront error are: 0.11 nm astigmatism; 0.58 nm coma; 0.8 nm sph ab; 0.18 nm trifoil; 1.13 nm 37-term RMS; 6.53 nm peak-to-valley. Gray scale ranges are (a) [−1.9, 2.6 nm], and (b) [−1.7, 2.7 nm].

cal aberration is subtracted from the comparison, the RMS difference is 0.79 nm, as shown in Fig. 1(b). Both measurements show similar contributions from the higher-order spherical aberration terms, with an EUV magnitude of 0.35 nm and a visible-light magnitude of 0.41 nm RMS. The astigmatism, and coma errors are close to zero in the visible-light data. The RMS difference magnitudes of a few important aberration components are: 0.11 nm astigmatism, 0.58 nm coma, 0.80 nm spherical aberration, 0.18 nm trifoil, 1.13 nm total RMS difference in a 37-term fit, and 6.53 nm peak-to-valley difference.

2. EUV alignment and stability concerns

System alignment was a primary task in the EUV measurement procedure. EUV LSI was used to for alignment feedback, with measurement and analysis requiring approximately 60 s. During the alignment iterations, performed to optimize the MET wavefront across the field of view, the alignment stability became an issue of concern at the level of 0.1–0.2 nm RMS, in the astigmatism, coma, and spherical aberration terms. Short term changes (mainly in coma and astigmatism) were observed in the minutes following alignment steps. More abrupt, unpredictable coma and spherical aberration changes were also detected in the hours following alignment; often these were 0.2–0.3 nm RMS in magnitude. For the latter cases, it appeared that the change would occur once and that the system would be stable afterward. In one case, a vent/pump cycle following alignment appears to have triggered a change in the alignment state despite the fact that venting (to nitrogen) occurred in a very slow, controlled manner.

3. EUV PS/PDI measurement and measurement comparison

Following the first system EUV alignment, the interferometer was changed into the PS/PDI configuration, requiring a vent. The PS/PDI measurements, performed during the next two days, showed a primary spherical aberration not present in the LSI measurements: a change of 0.36 nm RMS. After a thorough re-evaluation of the separate data analysis methods used in the LSI and the PS/PDI, we concluded that the observed measurements differences are likely not coming from differences in the analysis. We believe that the changes come from a discrete change in the system alignment state.

4. Final alignment and stability measurements

Before reconfiguration for EUV imaging, the system alignment was optimized for the last time on September 25, 2003. Aberration coefficients from that LSI field measurement are shown in Table I. The 37-term RMS wavefront error magnitude reached an optimized minimum value of 0.55 nm ($\lambda_{EUV}/24.5$) at the central field point.

The wavefront was measured several more times as the system sat virtually undisturbed for approximately one month. At one point during that period the temperature control system was accidentally deactivated for 12 h causing the chamber temperature to rise by 1 °C. We observed temperature-dependent changes in the wavefront as the system recovered its stable, 20.0 °C temperature set point. These wavefront changes are presumably due to transient temperature gradients in the optical housing, which affect the separation and possibly the relative angle of the mirrors. Even at the constant temperature, the wavefront aberrations, coma in particular, drifted away from the optimized state. Aberration coefficients from the final field measurement are shown in Table I labeled, "October 24, 2004." The 37-term RMS wavefront error magnitude at the central field point was 0.80 nm ($\lambda_{EUV}/16.9$). In the imaging configuration, we retain the ability to translate the field of view so that we may cover the region of the highest wavefront quality, if it has shifted.

5. Three-way comparison

Despite the alignment issues that cause uncertainties in the astigmatism, coma, and spherical aberration, a three-way comparison can be performed among the remaining aberration terms (Fig. 2). While the main purpose of the alignment is to minimize these three aberration terms, and removing them from consideration does eliminate the most important elements of the comparison, such a study reveals other differences between the measurements beyond the low-spatial-frequency alignment modes. In particular, the similarity in

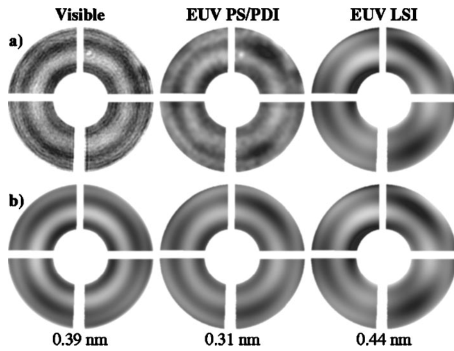

FIG. 2. Three-way comparison with alignment-dependent astigmatism, coma, and spherical aberration *removed* from consideration. (a) The phase maps contain the full spatial-frequency content of the original measurements (minus the alignment modes), which is different for each interferometer. (b) 37-term reconstructions on which the wavefront statistics are based. Gray scale range is $[-1.7, 2.0 \text{ nm}]$ for all wavefronts.

the higher-ordered spherical aberration measurement is evident; and between the two EUV measurements, very similar wavefront shapes are apparent. Yet there are clear differences between the visible-light and EUV measurements in the non-rotationally symmetric terms; and between the two EUV measurements, it appears that the LSI overestimates the aberration magnitudes by approximately 0.1 nm in this case.

6. Measurement precision

Repeated measurement of the system wavefront creates a large body of data that can be studied to determine the stability and repeatability of the interferometry itself. Such analysis is especially important in the presence of a suspected system alignment instability: To what extent can we be sure that we are not seeing differences brought on by the interferometry itself?

There are three primary ways to assess the repeatability of the LSI interferometry. The first is to calculate the *instantaneous repeatability* of the measurements; that is, when a series of sequential measurements are made, how self-consistent are the results? This measurement sets the upper limit of the repeatability that can be expected from other tests that take place over longer time spans. Analysis of hundreds of measurement sets consisting of 4–6 interferograms each, shows that the standard deviation of the individual aberration coefficients is 59 pm for astigmatism, 112 pm for coma, 17 pm for spherical aberration, and 54 pm for secondary coma. All other terms are below 32 pm, most are below 20 pm.

A second test of the measurement repeatability is the self-consistency of measurements made across the field. In these tests, different object pinholes and different regions of the grating beamsplitter are used. Furthermore, the entire optical system is translated by 3 mm during the measurements, which can take 2–4 h to perform. Data presented in Table I show that point-to-point variations are limited to a few hundred pm at most, and significantly smaller for most terms. Most of the relative, point-to-point variation is consistent with the other field measurements, arising from the natural aberration field dependence of the MET. Therefore, the combined effect of changing many measurement parameters is not larger than the differences we are attributing to alignment instability.

A third test of the measurement precision comes from the alignment process itself. As the system is aligned, step-by-step, measurements are made before and after every adjustment. Taking into account the uncertainties that accompany Picomotor-actuated adjustments on the scale from 30 nm to 2 μm, the results of arbitrary alignments were predictable to 100 pm, and often to better than 50 pm. This shows that the precision of the interferometric measurements is on par with or is better than those values.

III. SUMMARY

The measurements presented here demonstrate the successful application of at-wavelength interferometry to an EUV optical system with 0.3 NA. Using both LSI and PS/PDI, repeated measurements were made across the field of view during alignment optimization, in preparation for imaging. Interferometry and alignment brought the system to a diffraction-limited RMS wavefront error quality of 0.55 nm ($\lambda_{EUV}/24.5$) in a 37-term series. The wavefront error is dominated by a higher-order spherical aberration term that was predicted by visible-light measurements of the isolated M1 mirror and of the assembled system.

These measurements provide a rare and important opportunity for cross-comparison between visible-light and two EUV interferometry techniques. However, an apparent alignment drift complicated the alignment and the comparisons considerably. With the system at rest, only small, slow wavefront changes were observed over a period of days. However, measurements made before and after transportation from LLNL to LBNL, and also on several occasions at LBNL when the configuration of the interferometer was changed in a way that required a vent/pump cycle, show significant changes in spherical aberration and coma. Unknown changes to the alignment state thus compromise our ability to compare different wavefront measurement methods. Nonetheless, the visible-EUV comparison reached an agreement of approximately 1 nm, with good similarity in the higher-order spherical aberration measurement, but little agreement in the lowest-spatial-frequency terms, those associated with the system alignment. The EUV LSI-PS/PDI comparison showed agreement at the level of 0.57 nm RMS, or 0.46 nm when the primary difference, spherical aberration, was removed. These difference magnitudes represent a large fraction of the total wavefront error, leading us to the conclusion that the overall accuracy is thus far limited to approximately 0.5 nm. Improved shearing data analysis methods may improve the level of agreement between the two EUV techniques, and are the subject of ongoing research.

Following the final system alignment, the wavefront error magnitude at the central field point drifted upward slowly, reaching 0.80 nm ($\lambda_{EUV}/17$) after one month, yet maintaining "diffraction-limited" quality.

ACKNOWLEDGMENTS

This work would not have been possible without the hard work of the CXRO members, including Brian Hoef, Kevin Bradley, M. Gideon Jones, Ron Oort, Drew Kemp, Farhad Salmassi, René Delano, Al Rawlings, Ron Tackaberry, Robert Gunion, Hanjing Huang, Jeff Gamsby, Bruce Harteneck, and David Attwood. Additional thanks are due for the contributions of LLNL researchers including, John Taylor, Don Phillion, Layton Hale, Mike Johnson, Henry Chapman, Nhan Nguyen, Carl Chung, and Gary Sommargren. The authors are also indebted to Kim Dean of International Sematech and Pat Gabella of AMD for their support and guidance. This work is funded by the International Sematech, and by the U.S. Department of Energy.

[1] R. Hudyma, Information Science and Technology Program, Internal Report, September 24, 1999, M199900286.
[2] K. A. Goldberg, P. Naulleau, P. Denham *et al.*, Proc. SPIE **5037**, 69 (2003).
[3] K. A. Goldberg, P. Naulleau, P. Denham *et al.*, J. Vac. Sci. Technol. B **21**, 2706 (2003).
[4] P. Naulleau, K. Goldberg, P. Batson, J. Bokor, P. Denham *et al.*, Appl. Opt. **42**, 820 (2003).
[5] K. A. Goldberg, P. Naulleau, J. Bokor, and H. N. Chapman, Proc. SPIE **4688**, 329 (2002).
[6] P. Naulleau, K. A. Goldberg *et al.*, J. Vac. Sci. Technol. B **19**, 2396 (2001).
[7] P. Naulleau, K. Goldberg, E. Gullikson, and J. Bokor, Appl. Opt. **39**, 2941 (2000).
[8] J. E. M. Goldsmith, K. W. Berger, D. R. Bozman *et al.*, Proc. SPIE **3676**, 264 (1999).
[9] S. A. Robertson, P. P. Naulleau, and K. A. Goldberg, Proc. SPIE **5037**, 900 (2003).
[10] P. P. Naulleau, K. A. Goldberg, and J. Bokor, J. Vac. Sci. Technol. B **18**, 2939 (2000).
[11] P. P. Naulleau, K. A. Goldberg, S. H. Lee, C. Chang *et al.*, Appl. Opt. **38**, 7252 (1999).
[12] M. P. Rimmer, Appl. Opt. **13**, 623 (1974).
[13] G. Harbers, P. J. Kunst, and G. W. R. Leibbrandt, Appl. Opt. **35**, 6162 (1996).
[14] H. van Brug, Appl. Opt. **36**, 2788 (1997).